Ligand Exchange of Au25SG18 Leading to Functionalized Gold Clusters: Spectroscopy, Kinetics, and Luminescence

4 AUTHORS, INCLUDING:

Elizabeth Shibu
Dubai Health Authority
7 PUBLICATIONS **232** CITATIONS

SEE PROFILE

Habeeb Muhammed Madathumpady Abub…
Ludwig-Maximilians-University of Munich
14 PUBLICATIONS **855** CITATIONS

SEE PROFILE

Pradeep Thalappil
Indian Institute of Technology Madras
347 PUBLICATIONS **8,810** CITATIONS

SEE PROFILE

Article

Ligand Exchange of AuSG Leading to Functionalized Gold Clusters: Spectroscopy, Kinetics, and Luminescence

E. S. Shibu, M. A. Habeeb Muhammed, T. Tsukuda, and T. Pradeep

More About This Article

Additional resources and features associated with this article are available within the HTML version:

- Supporting Information
- Access to high resolution figures
- Links to articles and content related to this article
- Copyright permission to reproduce figures and/or text from this article

View the Full Text HTML

Ligand Exchange of Au₂₅SG₁₈ Leading to Functionalized Gold Clusters: Spectroscopy, Kinetics, and Luminescence

E. S. Shibu,[†] M. A. Habeeb Muhammed,[†] T. Tsukuda,[‡] and T. Pradeep*,[†]

DST Unit on Nanoscience (DST UNS), Department of Chemistry and Sophisticated Analytical Instrument Facility, Indian Institute of Technology, Madras, Chennai 600 036, India and Institute for Molecular Science, Myodaiji, Okazaki 444-8585, Japan

Ligand exchange offers an effective way to modify the properties of the recently prepared quantum clusters of gold. To tune optical and photoluminescence properties of one of the most stable quantum clusters of gold, Au₂₅SG₁₈ (SG-glutathione thiolate), we functionalized it by the exchange of −SG with functionalized -SG and with an altogether different ligand, namely, 3-mercapto-2-butanol (MB). The products were characterized by various techniques such as optical absorption (UV−vis), Fourier-transform infrared (FT-IR), nuclear magnetic resonance (NMR), X-ray photoelectron (XPS), and luminescence spectroscopies, mass spectrometry, and thermogravimetry (TG). Analyses of the TG data helped to establish the molecular composition of the products. Ligand exchange reaction was monitored by NMR spectroscopy, and it was found that the exchange reaction follows a first order kinetics. The XPS study showed that after the exchange reaction there was no change in the chemical nature of the metal core and binding energy values of Au 4f₇/₂ and 4f₅/₂, which are similar in both the parent and the exchanged products. Photoluminescence studies of these clusters, done in the aerated conditions, showed that the excitation spectrum of the MB-exchanged product is entirely different from the acetyl- and formyl-glutathione exchanged products. The inherent fluorescence and solid-state emission of these clusters were observed. This intense emission allows optical imaging of the material in the solid state. The emission is strongly temperature dependent. The synthesis of a diverse variety of clusters and their chemical stability and intense luminescence offer numerous applications in areas such as energy transfer, sensors, biolabeling, and drug delivery.

Introduction

Gold nanoparticles are the subject of intense research for the past few years. Versatile synthetic approaches have been developed to prepare size-controlled particles in large yield.[1,2] Evolution in the synthetic approaches have made it possible to get particles of diverse shapes such as rods, triangles, prisms, plates, stars,[3–8] etc. Along with these synthetic techniques, molecular quantum clusters of metals are also prepared.[9,10] Nanoclusters are a new class of materials that are made up of tens to hundreds of atoms and have intermediate composition between bulk and molecular regimes, where electronic band structure of the bulk gets modified to discrete electronic states as a result of quantum confinement. Metal nanoclusters are of considerable interest because of their distinct size dependency in electronic properties. Nanoclusters with diameters less than 2 nm show discrete electronic transitions among the quantized levels, which can be useful in nanoelectronics,[11] sensing applications,[12–14] catalysis,[15,16] and bioanalysis.[17] Synthesis of Au₁₁,[18] Au₅₅,[19] and Au₈[20] are significant developments in cluster science. Among these, water-soluble, monodisperse, blue-emitting Au₈ nanodots encapsulated in biocompatible second and fourth generation −OH terminated poly(amidoamine) (PAMAM, G2-OH and G4-OH) dendrimers, exhibit a fluorescence quantum yield of 41%, more than 100-fold enhancement over other reported gold nanoclusters. Au₈ clusters, as well as

other clusters such as Au₅, Au₁₃, Au₂₃, and Au₃₁, were also encapsulated in the PAMAM cavity, and these PAMAM-encapsulated differently sized nanodots exhibit discrete excitation and emission spectra from the ultraviolet to near-infrared region.[21]

A series of glutathione thiolate (SG-thiolate) protected gold clusters with well-defined compositions were synthesized and separated utilizing polyacrylamide gel electrophoresis (PAGE).[22] The molecular compositions of these clusters were characterized by electrospray ionization (ESI) mass spectrometry. The isolated clusters include Au₁₀SG₁₀, Au₁₅SG₁₃, Au₁₈SG₁₄ Au₂₂SG₁₆, Au₂₂SG₁₇, Au₂₅SG₁₈, Au₂₉SG₂₀, Au₃₃SG₂₂, and Au₃₉SG₂₄. Although this approach provides a versatile method of synthesizing thiolated gold clusters, major drawbacks were the poor yield and the cumbersome procedure to get usable quantities, as it involves PAGE. The ligand exchange reaction of phosphine-stabilized gold clusters (Au₁₁) with GSH gave only Au₂₅SG₁₈ in large yield suggesting that the Au₂₅ cluster is the most stable one among the thiolated clusters of this class.[23] It is well-known that magic numbered clusters can be preferentially populated by the successive removal of the precursors from the outer layer.[24] So if one can sequentially remove the Au atoms from the outer layers of the preformed Au−SG nanoparticles, then it is possible to create certain stable clusters among this class. One of the versatile methods for core-size reduction of Au@SG clusters is chemical etching with free thiols. Recently, Au@SG clusters were chemically etched with free glutathione; it was found that Au₂₅SG₁₈ exhibits an extraordinary stability against core etching.[24] Using this core-size reduction method,

* Corresponding author. Fax: + 91-44 2257-0545. E-mail: pradeep@iitm.ac.in
† Indian Institute of Technology.
‡ Institute for Molecular Science.

Ligand Exchange of Au$_{25}$SG$_{18}$

J. Phys. Chem. C, Vol. 112, No. 32, 2008 **12169**

Au$_{25}$SG$_{18}$ clusters were synthesized in gram scale from the crude Au@SG, containing a mixture of clusters. The incorporation of suitable molecules can add desired properties to these molecular clusters. As molecular quantum clusters belong to a subclass of monolayer protected clusters, they are studied extensively by various groups. One important means by which monolayer protected clusters (MPCs) can be functionalized is through ligand exchange, pioneered by Murray and co-workers.[25] By ligand exchange, a selective functionality is incorporated onto the MPC by exchanging the monolayers with desired molecules containing appropriate functional groups.

We explored different substitution reactions of glutathione clusters of gold and investigated various aspects of this chemistry using spectroscopic techniques. One of our principal objectives was to modify the optical and photoluminescence properties of this cluster. Luminescence from a metal surface has very low efficiency. In the case of semiconductors, an electronic excitation from the valance band to the conduction band will initially decay through a nonradiative path until the system reaches the lowest possible state of the conduction band. Transitions across the band gap are radiative, if allowed. In the case of metals, all the energy of the excitation gets dissipated via nonradiative processes. However, one can expect to see photoluminescence from a metal if an energy gap is present among the higher-lying states. Photoluminescence studies conducted on nanometer-sized gold clusters assigned the near-infrared (NIR) transitions to sp or sp-like transitions, analogous to intraband transitions in bulk gold.[26,27] Au$_{25}$SG$_{18}$, the most stable among all the nine fractions of crude Au@SG, shows a photoluminescence band in the near-infrared (NIR) region when excited at 530 nm.

Recently, Murray and co-workers reported[28] the crystal structure of [Au$_{25}$(SCH$_2$CH$_2$Ph)$_{18}$$^-$] [TOA$^+$]. It has been found that the molecule has three types of gold atoms; one is at the center, 12 form the vertices of the icosahedron around the central atom, and the remaining 12 gold atoms are stellated on 12 of the 20 faces of the Au$_{13}$ icosahedron. The icosahedral Au$_{13}$ core is protected by six (−SR−Au−SR−Au−SR−) cyclic oligomers. Two sulfur environments are observed in the structure, 6 of one kind and 12 of another. Density functional theory (DFT) supports the structure of Au$_{25}$ clusters.[29] The proposed theoretical structure is based on a compact icosahedral Au$_{13}$ core with a protection of six MeS−Au−MeS−Au−MeS complexes. The structure proposed earlier[30] is found to be a metastable isomer.

In this article, we report the exchange of glutathione ligands of Au$_{25}$SG$_{18}$ clusters in two different ways. In the first case (type 1), we used an entirely different water soluble thiol, namely, 3-mercapto-2-butanol (MB) for the exchange with −SG. In the second case (type 2), we used functionalized GSH; N-acetyl- and N-formyl-glutathione (NAGSH and NFGSH, respectively). Exchange with these ligands was tried because direct synthesis of Au$_{25}$ with these ligands was unsuccessful. The exchanged products were characterized by UV−vis, FT-IR, ^{1}H NMR, X-ray photoelectron spectroscopy (XPS), thermogravimetric analysis (TG), LC/MS/MS mass spectrometry, and fluorescence spectroscopies. Kinetics of the exchange reaction was monitored by time-dependent ^{1}H NMR spectroscopy. Kinetic studies revealed that the −SG ligands are not completely replaced by MB and that the reaction is over within 3 h. It is clear that some of the Au centers are labile and that others are inert toward the exchange of MB. XPS study showed that after the exchange reaction there is no change in the chemical nature of the metal core, since binding energy values of Au 4f$_{7/2}$ and 4f$_{5/2}$ are similar in both the parent and the

exchanged products. Parent Au$_{25}$SG$_{18}$ cluster shows an emission maximum at 700 nm (excited at 530 nm), which was retained in the exchanged products, suggesting that the core size of the exchanged products is the same as that of the parent clusters. However, the excitation spectrum of the MB-functionalized Au$_{25}$ cluster shows a blue shift of 20 nm.

Experimental Section

Materials and Methods. *Materials.* All the chemicals were commercially available and were used without further purification. HAuCl$_4$·3H$_2$O, methanol (GR grade), ethanol (GR grade), and GSH (γ-Glu-Cys-Gly, MW = 307) were purchased from SRL Chemical Co. Ltd., India. NaBH$_4$ (>90%) and MB (MW = 106) were purchased from Sigma Aldrich. Acylation and formylation of GSH were performed using the reported procedure.[31] Deionized water with a resistivity of >18 MΩ cm was used for all experiments. All the product names are abbreviated as Au$_{25}$SG$_{18}$, Au$_{25}$−MB, Au$_{25}$−SGAN, and Au$_{25}$−SGFN, respectively.

Synthesis of Au@SG. To a 50 mL methanolic solution of (0.25 mM) HAuCl$_4$·3H$_2$O, 1.0 mM GSH was added (1:4 ratio, total volume of methanol was 50 mL). The mixture was cooled to 0 °C in an ice bath for 30 min. Then, an aqueous solution of NaBH$_4$ (0.2 M, 12.5 mL), cooled to 0 °C, was rapidly injected into the above mixture under vigorous stirring. The mixture was allowed to react for another hour. The resulting precipitate was collected and repeatedly washed with methanol through centrifugal precipitation. Finally the Au@SG precipitate was dried and collected as a dark brown powder.[22]

Synthesis of Au$_{25}$SG$_{18}$ from Crude Au@SG. The above powder was dissolved in 50 mL of 1.0 mM SG (in water) and heated at 55 °C (±5 °C) in a round-bottom flask for about 12 h.[32] The solid material formed was centrifuged out and from the solution; Au$_{25}$SG$_{18}$ was precipitated from the solution by the addition of methanol; the precipitate was then repeatedly washed with methanol and finally with ethanol. The precipitate was dried in vacuum and giving a brown powder. The material was stored in the dry form in the refrigerated condition. Fresh solutions were prepared for all studies. However, in general, the solutions are found to be stable for periods on the order of weeks. It is known that Au$_{25}$ is the most stable among the clusters formed.[24]

Exchange Reactions. *Exchange Reaction with MB (Type 1).* To a water solution of Au$_{25}$SG$_{18}$ (2.5 mg/mL), MB (0.46 μL/mL) was added, and the mixture was stirred for 3 h at room temperature. The exchanged product was precipitated using ethanol and then dried to yield a black-brown powder. Schematic representation of the exchange reactions is shown in Scheme 1.

Exchange Reaction with NAGSH and NFGSH (Type 2). To approximately 20 mg of Au$_{25}$SG$_{18}$ in 5 mL of distilled water, 10.6 mg each of N-acetyl- or N-formyl-glutathione were separately added and stirred for 3 h at room temperature. The exchange product was precipitated using ethanol and was dried to yield a black brown powder. From independent experiments it was found that the exchange was complete within this period. The materials prepared were as stable as the parent materials in the solid and solution states.

Methods. UV−vis spectra were recorded using a Perkin-Elmer Lambda 25 spectrometer. Infrared spectra were recorded using a Perkin-Elmer Spectrum One spectrometer. Samples were made in the form of dispersed (5%) KBr pellets. KBr crystals were used for all the measurements to avoid water and other organic impurities. Spectra were collected at a resolution of 4 cm^{-1}. ^{1}H NMR was recorded using a Bruker 400 MHz

SCHEME 1: Schematic Representation of the Exchange Reactions[a]
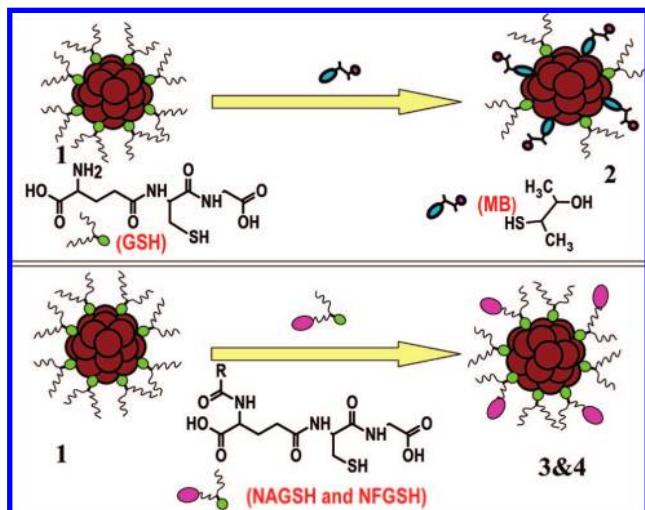
[a] Structures of the ligands used are also shown.

instrument. The photoexcitation and fluorescence studies were done using a Hitachi F-4500 spectrofluorimeter with a 100 W xenon lamp as the excitation source at a scan speed of 240 nm/ sec. The band pass for both excitation and emission monochromators was kept at 5 nm. The experimentally obtained intensities in absorbance and emission, as a function of wavelength [$I(W)$], have been converted to energy-dependent values [$I(E)$] using the expression $I(E) = I(W)/(\partial E/\partial W) \propto I(W) \times W^2$, where $\partial E/\partial w$ represents the Jacobian factor. Solid-state emission and inherent fluorescence images were measured using a Witec GmbH confocal Raman spectrometer equipped with a 514.5 nm excitation. The excitation laser was focused using a 100× objective, and the signal was collected in a back-scattering geometry and guided to a Peltier-cooled charge coupled device (CCD) detector. The sample was mounted on a piezo-equipped scan stage to enable spectral imaging. Spectral intensities acquired over a predefined area were automatically compared to generate color-coded images. In the images, regions coded yellow are regions with maximum fluorescence intensities, and regions shown in black are those with minimum signal intensities. Temperature-dependent fluorescence data were collected with an Oxford cryostat mounted on the Raman spectrometer, and lower temperatures were obtained by liquid nitrogen circulation. Thermogravimetric (TG) analysis was done using a Perkin-Elmer Diamond TG/DTA with a sensitivity of 0.2 μg. Samples were loaded in milligram scale and were heated from room temperature to 800 °C at a heating rate of 5 °C per minute in air. X-ray photoelectron spectroscopy (XPS) measurements were done using a VG Microtech Multilab ESCA 3000 spectrometer with non-monochromatized Al K$_\alpha$ X-rays ($h\nu$ = 1486.6 eV). At least ten spectra in the desired binding energy range were collected, and an average was taken. The samples were spotted as drop cast films on the sample stub, and the surface was scraped in situ to remove any surface contamination that could arise from components of the atmosphere such as water and CO_2. X-ray flux was adjusted to reduce the beam-induced damage of the sample. The energy resolution of the spectrometer was set at 1.1 eV at a pass energy of 50 eV. Binding energy (BE) was calibrated with respect to C1s (285 eV). TEM images were collected using a JEOL 3010 microscope. Samples were spotted from diluted solutions on carbon coated copper grids and were dried at room temperature. Images were collected at 200 keV. Intense electron beam irradiation,

even for short periods, causes significant aggregation and fusion of the nanoclusters, and larger particles were formed. Particles were examined for shorter periods in the form of well-dispersed films. The mass spectrometric studies were conducted using an electrospray system, 3200 Q-TRAP LC/MS/MS (Applied Biosystems). A 15 ppm solution of the quantum clusters was electrosprayed. Because the spray is orthogonal to ion extraction in this instrument, it is known from the earlier report[22] that only certain fragments such as $[Au(SG)_2-H]^{-1}$ ($m/z = 808$) and $[Au_2(SG)_2-H]^{-1}$ ($m/z = 1005$) are detectable. The spectra showed only the features due to the monolayers and smaller Au clusters in all the samples. These data are especially useful for characterization when substitution is done and when the clusters are functionalized.

Results and Discussion

All exchange products appeared very similar to the parent $Au_{25}SG_{18}$. They had very high solubility in water, as in the case of $Au_{25}SG_{18}$, although substituted ligands have significantly different solubility in comparison to GSH. The ligand exchanged products were stable, and the solutions did not show decomposition in the laboratory atmosphere for periods extending over several months. Direct syntheses of Au_{25} with these ligands (following the protocol used for GSH) were unsuccessful. Similarly, repeated exchange to make completely ligand-exchanged products was also unsuccessful. The difficulty involved in directly synthesizing $Au_{25}L_{18}$ (L = MB, NAGSH, and NFGSH) may be attributed to the limited understanding of the details of cluster formation. Both Au(I) and Au(0) species are required for cluster formation, if one were to consider direct growth from solution. If the cluster is prepared by ligand etching, then careful control of the synthetic parameters is required to retain the Au_{13} core with appropriate thiolate protection. The species involved in etching and the type of surface species etched away become important. It is unlikely that solubility of these ligands is the reason for the unsuccessful synthesis of Au_{25} with them. As Au_{25} with GSH and SCH_2CH_2Ph ligands have been synthesized,[22–24,28,32,33] it is clear that the core is likely to be stable with a complete cover of the present set of ligands as well. Therefore, the unfeasible synthesis of Au_{25} with these ligands can only imply that the core etching route for the formation of Au_{25} is unsuccessful with them. A more careful manipulation of the experimental conditions may be necessary to stabilize $Au_{25}L_{18}$ systems.

The clusters have the same core diameter (0.7 nm) as the parent $Au_{25}GS_{18}$ and are extremely sensitive to the electron beam. Upon longer exposure at 200 keV, the cores coalesce to yield nanoparticles. The HRTEM data of the clusters and their conversion to larger nanoparticles upon electron beam exposure are shown in Supporting Information (Figure S1). As a result, the cluster characterization has to depend exclusively on spectroscopic techniques. Because mass spectrometry of Au_{25} clusters has been discussed before, we present only additional details, especially those of relevance to this work. Electrospray ionization MS with mass detection orthogonal to the electrospray is unable to detect the clusters in their native state as mentioned above. An orthogonal ESI-MS mass spectrum gives characteristic peaks at m/z 808 and 1005, which are in good agreement with that reported earlier. The ESI spectrum is given in the Supporting Information (Figure S2).

Electronic absorption spectra of the quantum clusters show rich features attributed to molecular transitions. The absorption at 672 nm is due to the intraband transition (HOMO−LUMO) derived from sp orbitals of Au. This position is characteristic
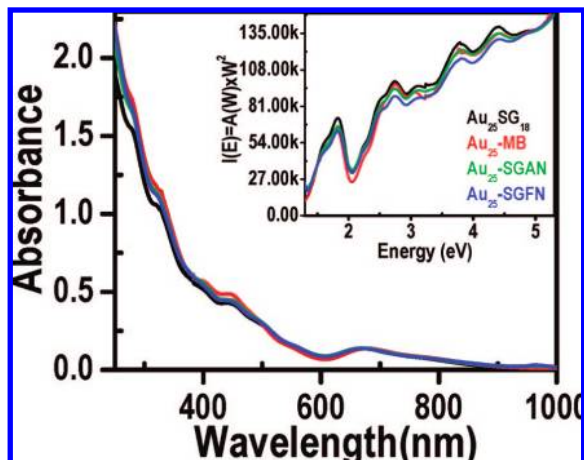
Figure 1. The UV−vis spectra of compounds $Au_{25}SG_{18}$ (black), Au_{25}−MB (red), Au_{25}−SGAN (green), and Au_{25}−SGFN (blue). Inset shows the plot of $I(E) = A(W) \times W^2$ vs energy (eV).

of Au_{25} clusters and occurs in all Au_{25} molecules reported so far.[22–24,32,33] In conformity with these reports, various samples reported here show the same features. All of them show the HOMO−LUMO transition at 672 nm. Each and every minor feature of Au_{25} is reproduced in the ligand exchanged products. Figure 1 shows the UV−vis spectra of Au_{25} and the exchanged products. These spectra were normalized with respect to the HOMO−LUMO transition. However, minor changes are observed for the transitions at 274, 316, and 444 nm, implying that only these have mixed ligand−metal character. The inset shows the plot $I(E) = A(W) \times W^2$ versus energy (eV). Although the UV−vis spectrum of the type 2 exchanged products did not show any change in the intraband transition, the type 1 product showed a slight red shift of 10 nm. We propose that this effect is due to the solvent because the core in Au_{25}−MB can interact with the solvent more closely due to the shorter

chain length. The peak at 444 nm is distinctly different for Au_{25}−MB, but in all others it is very similar. Calculations suggest that the absorption spectrum does not show ligand dependence, and our results are fully in accordance with this.[30] This is especially true of the HOMO−LUMO transitions, as these are due to the compact icosahedral Au_{13} core.

FT-IR spectra of all the ligands and exchanged products are shown in Figure 2. Each ligand is compared with the corresponding cluster. A characteristic aspect of the spectrum is the complete disappearance of the SH stretching at $\sim$2557 cm^{-1} (marked by circle). This is particularly noticeable in $Au_{25}SG_{18}$, Au_{25}−MB, and Au_{25}−SGAN. In the case of the formyl analogue (Au_{25}−SGFN), the SH stretching band is not pronounced in the ligand. The presence of these exchanged ligands is evident in the IR spectra. MB substitution is manifested in terms of well-defined OH features, which underwent blue shift in comparison to the parent molecule (marked by dashed line). This is likely to be due to the absence of pronounced hydrogen bonding in the substituted product, in comparison to the free ligand. This is expected because the ligands are likely to be located at different positions on the Au_{25} surface. The presence of MB is also manifested by the −CH$_3$ stretching band at 2975 cm^{-1}, which occurs at the same position as in the case of the parent ligand. In the acetyl analogue (Au_{25}−SGAN), −CH$_3$ features appear at 2935 cm^{-1}. The fingerprint regions of the spectra are similar for $Au_{25}SG_{18}$, Au_{25}−SGAN, and Au_{25}−SGFN but differences are noticeable in the case of Au_{25}−MB. Expanded views of the spectra are given in the Supporting Information (Figure S3), where these difference are easily observable.

^{1}H NMR of pure GSH shows five characteristic peaks, and these are assigned *a−f* in Figure 3. Glutathione is a tripeptide consisting of three amino acids, namely glutamic acid, cysteine, and glycine. The peaks at 2.2 (*e*), 2.5 (*d*), and 4 (*f*) ppm correspond to the γ −CH$_2$, β −CH$_2$, and β −CH of glutamic acid, respectively.[34] Peaks at 3 (*c*) and 3.8 (*a, b*) ppm are due
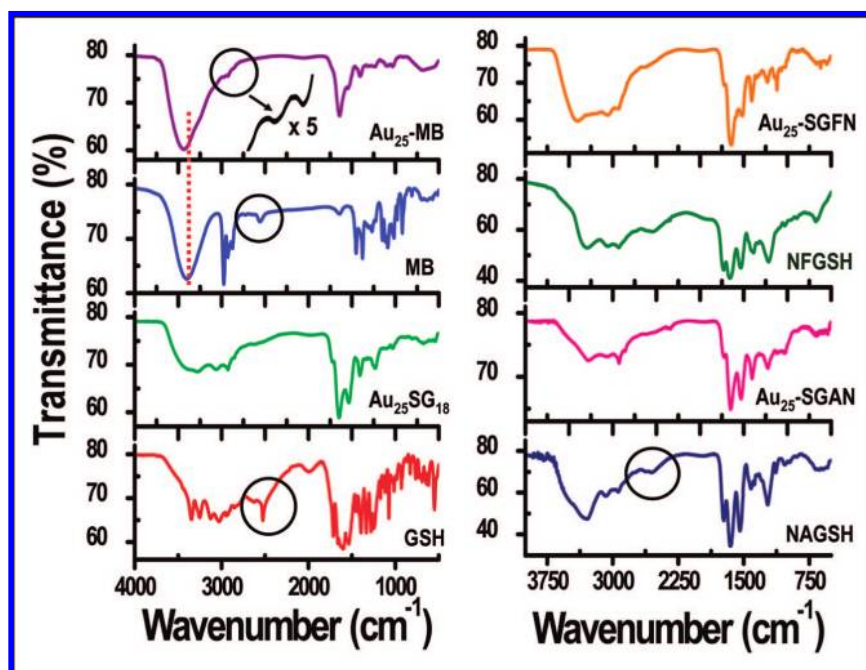
Figure 2. FT-IR spectra of pure GSH, Au25SG18, MB, Au25−MB, NASGH, Au25−SGAN, NFSGH, and Au25−SGFN. The −SH stretching features in the ligands are marked by circles. NFGSH does not prominently show the −SH stretching feature. The shift of the −OH peak of Au25−MB is compared with that of the parent ligand, and it is marked by the dashed line. The expanded view of the −CH3 stretching region of Au25−MB is shown (shifted in *x*-axis).
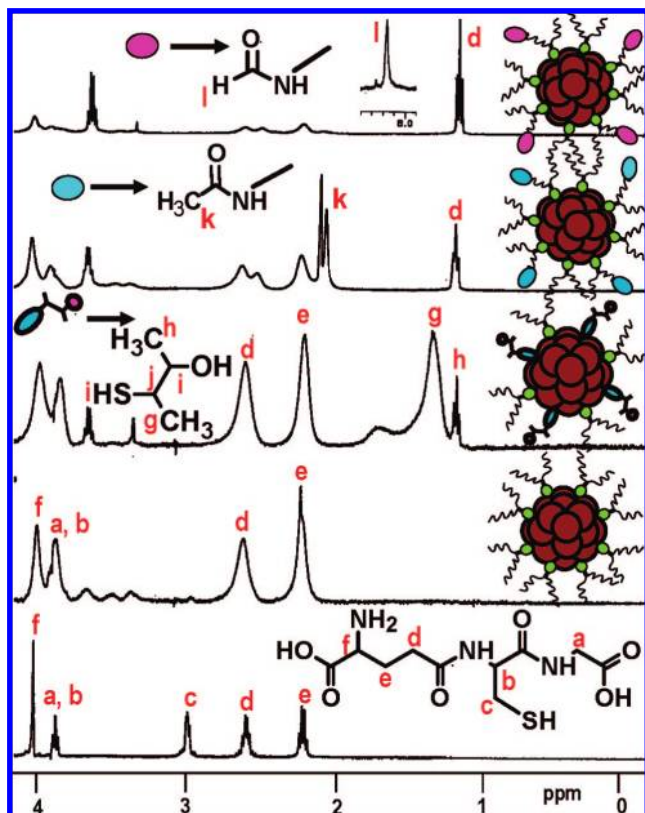
Figure 3. ^{1}H NMR spectra of GSH and products—Au$_{25}$SG$_{18}$, Au$_{25}$–MB, Au$_{25}$–SGAN, and Au$_{25}$–SGFN. Note that there is one-to-one correspondence between the spectrum of GSH and Au$_{25}$SG$_{18}$, except that the resonance due to the β –CH$_2$ of cysteine has completely disappeared.

to the α –CH$_2$ and α –CH of cysteine. The peak of α –CH of glycine occurs at 3.8 ppm, hence it is merging with the α –CH of cysteine. The ^{1}H NMR of glutathione-capped Au$_{25}$ shows all the characteristic peaks of the glutathione moiety, but they are significantly broadened. In the ^{1}H NMR of the Au$_{25}$SG$_{18}$ cluster, the peak corresponding to β –CH$_2$ of cysteine (*c*) almost completely disappeared since it is very close to the gold surface. Near complete disappearance of α –CH resonance is seen in MPCs protected with alkanethiols.[35]

We confirmed the ligand exchange by ^{1}H NMR spectroscopy (Figure 3). The broadening of the peak at 1.35 ppm (corresponding to the –CH$_3$ near to the –SH of the MB) and the disappearance of the peak at 3 ppm (corresponding to the –CH near to the –SH of MB) are strong evidences for the presence of bound MB on the Au$_{25}$ cluster. In the case of Au$_{25}$–SGAN, the acetyl –CH$_3$ proton comes in around 2.3 ppm (*k*). The peak at 8.2 ppm (*l*) shows the presence of the formyl group in these Au$_{25}$ clusters. The expanded ^{1}H NMR spectra of all the exchanged products and their corresponding analogous are given in the Supporting Information (Figure S4).

The exchange reaction was monitored using time-dependent ^{1}H NMR spectroscopy (Figure 4a). The spectra were recorded at an interval of 30 min. From the spectra we can say that as the time progresses, the features of the free GSH molecule are increasing in intensity compared to the bound one (marked in the figure). The emergence of free GSH features in ^{1}H NMR clearly shows the substitution of –SG groups by MB molecules. In the ^{1}H NMR spectrum (Figure 3), the peaks at 2.9, 2.6, and 2.25 ppm are due to the β –CH$_2$ of cysteine, γ –CH$_2$ of glutamic acid, and β –CH$_2$ of glutamic acid, respectively. The peaks corresponding to the *d* and *e* protons are of interest to the time-dependent ^{1}H NMR studies, because these show
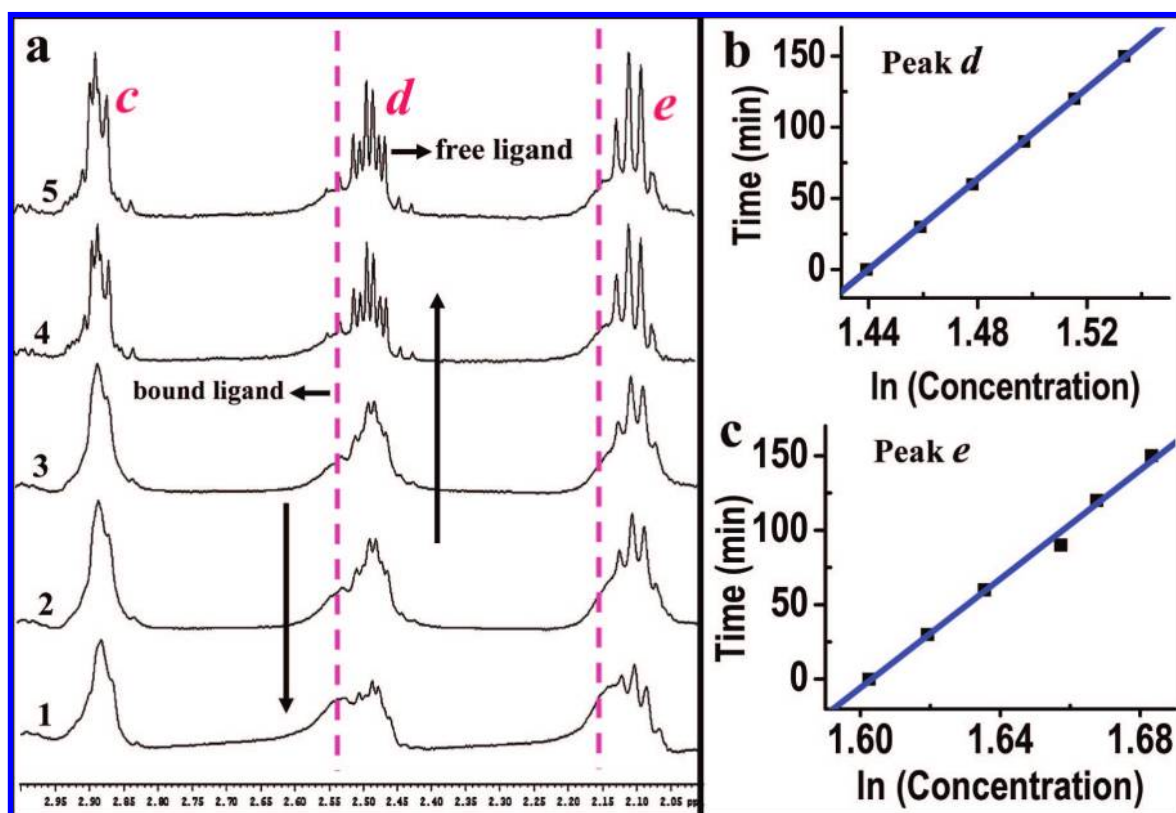

Figure 4. (a) The time-dependent ^{1}H NMR spectrum of the exchange reaction of MB with Au$_{25}$SG$_{18}$. Spectra 1–5 correspond to the time intervals of 0, 30, 60, 90, 120, and 150 min, respectively. The graphs b and c are plots of time vs ln(concentration) for the peaks corresponding to *d* and *e*, respectively. Because the intensities are proportional to concentration, the *x*-axis in b and c are labeled as ln(concentration).

Ligand Exchange of Au$_{25}$SG$_{18}$

*J. Phys. Chem. C, Vol. 112, No. 32, 2008* **12173**

systematic changes as the reaction progressed. With increasing time of exchange, broadening of these peaks gets reduced, and the characteristic multiplicity seen in the case of the pure ligand (GSH) appears. However, the peaks are still broadened, because a few −SG groups are attached to the cluster surface. Moreover, due to the time it takes to measure the spectrum, we could not take the spectrum at zero time (immediately after mixing the reagents) and hence the first measurement itself shows the presence of β −CH$_2$ of cysteine at 2.9 ppm. Note that this peak does not appear in the spectrum of the parent cluster (Figure 3). We have taken the intensities of the first measurement as due to zero time and computed the integrated intensities for the *d* and *e* peaks. Because the integrated intensities of the peaks are directly proportional to the concentration, we plotted the time against logarithms of these values, and the data are in good agreement with first order kinetics (Figure 4, panels b and c). The rate constant calculated is 1.3×10^{-4} sec^{-1}. As the β −CH$_2$ is very close to the cluster surface, additional relaxation broadens it to the baseline in the bound cluster. Because of this, its intensity was not considered in the evaluation of kinetic parameters. The limited range of concentrations is due to the fact that satisfactory intensities for both the constituents could be observed in this window.

Figure 5 shows the Au 4f core level photoemission spectra of products Au$_{25}$SG$_{18}$, Au$_{25}$−MB, and Au$_{25}$−SGAN. Because the chemical nature of the compounds Au$_{25}$−SGAN and Au$_{25}$−SGFN are similar, the latter was not examined. The 4f features were similar in all the cases, implying that the cluster core did not undergo any change after the exchange reactions. The BE positions and width are similar in all the cases. The C1s and N1s regions were also examined, and these also showed similar results, which are given in Supporting Information (Figure S5). Observed binding energy values are close to those reported before[22] with Au 4f$_{7/2}$ at 84 eV and Au 4f$_{5/2}$ at 88 eV. These data suggest that the cluster cores are similar in all of these cases.

Photoluminescence (PL) spectra of compounds Au$_{25}$SG$_{18}$, Au$_{25}$−MB, Au$_{25}$−SGAN, and Au$_{25}$−SGFN were recorded in aqueous solutions at room temperature. All measurements were conducted in aerated conditions. The cluster concentrations for the PL measurements were typically milligram per milliliter, where the PL intensities increase linearly with the cluster concentrations. PL spectra (Figure 6) are distinctly different only in the case of MB-substituted products, where the excitation
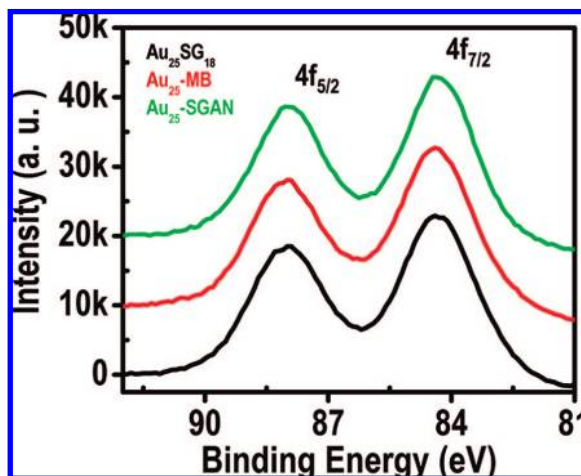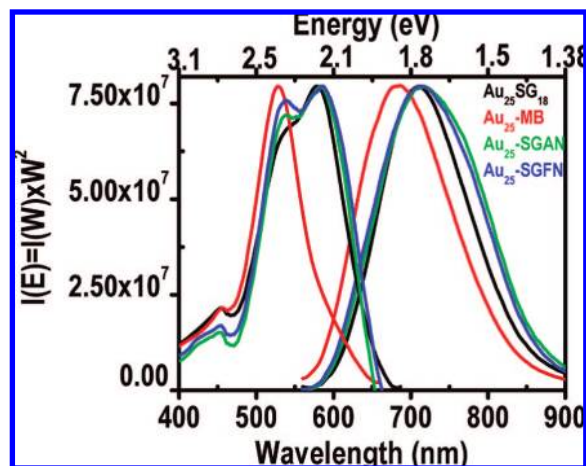
Figure 6. Photoexcitation and emission spectra of compounds Au$_{25}$SG$_{18}$, Au$_{25}$−MB, Au$_{25}$−SGAN, and Au$_{25}$−SGFN. Intensity plotted is $I(W) \times W^2$.
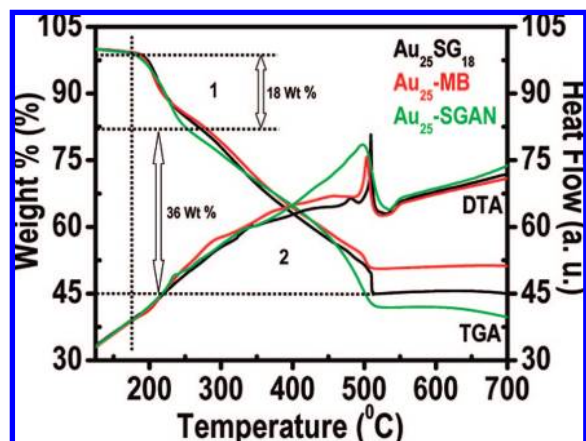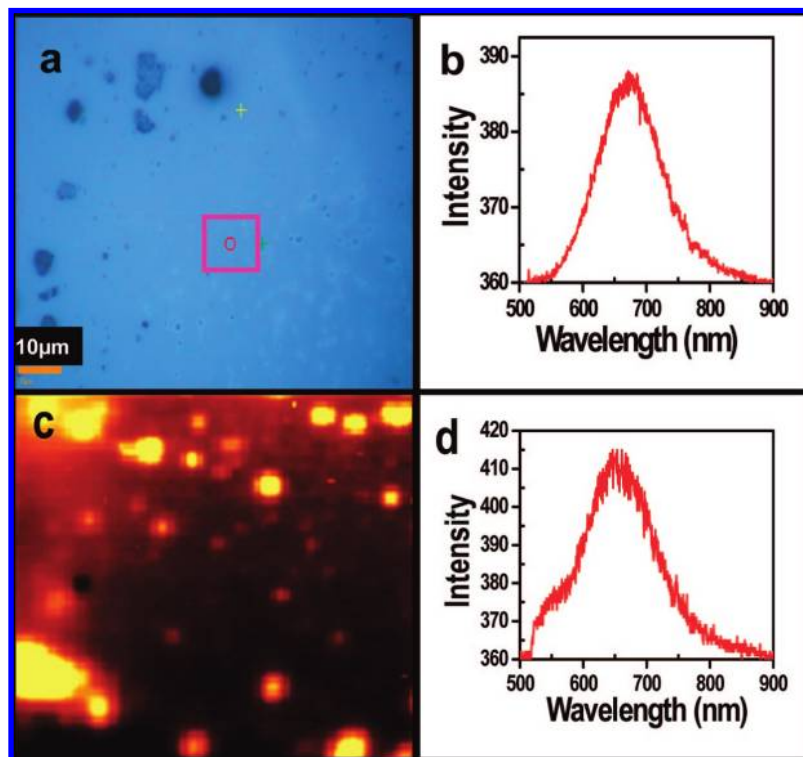

Figure 7. TG curves of compounds Au$_{25}$SG$_{18}$, Au$_{25}$−MB, and Au$_{25}$−SGAN. The two steps in desorption are indicated by dotted lines. The DTA traces are also shown. The various regions of mass losses for Au$_{25}$SG$_{18}$ are labeled. The mass percentages shown are approximate values because well-defined mass losses are not seen.

spectrum shows only one maximum at 527 nm (2.3 eV), which also shows a blue shift of 20 nm, whereas in all the other clusters a doublet was observed at 2.15 and 2.30 eV, in agreement with the earlier report.[22] Comparing with the absorption spectrum, it is this region where MB-substituted product differs from other clusters. Out of the three functionalized clusters, Au$_{25}$−MB shows a difference in the excitation−emission spectrum even though a few ligands were replaced. Therefore, it appears that one can tune the photoluminescence of Au$_{25}$ clusters, although slightly, by choosing proper water-soluble ligands. The PL maximum of Au$_{25}$SG$_{18}$ is slightly different from the reported values,[22] and it could be due to the reduced sensitivity of the detector at high wavelength. Quantum clusters of gold have been investigated in detail using luminescence spectroscopy.[36] NIR emission is observed in several of them, and Au$_{25}$ is not different. The data clearly established that this emission is an inherent property of the core, and the same electronic transitions can be accessed for a variety of ligands. Although the excitation spectrum could be modified, emission always occurs between the same energy levels, implying that they are metal derived. This suggestion is supported by calculations that suggest metal-derived valence states,[30] as mentioned previously.

Thermogravimetric (TG) analysis of compounds Au$_{25}$SG$_{18}$, Au$_{25}$−MB, and Au$_{25}$−SGAN were performed in static air. TG

Figure 5. The Au 4f core level photoemission spectra of compounds Au$_{25}$SG$_{18}$, Au$_{25}$−MB, and Au$_{25}$−SGAN. The traces have been shifted vertically.

Figure 8. (a) Optical image; (b) solid-state emission of $Au_{25}SG_{18}$; (c) inherent fluorescence image collected by the spectroscopic mapping of an area of 15×15 μm, represented by the box in panel a; and (d) solid-state emission from $Au_{25}-MB$. The images and spectra were collected with 514.5 nm excitation.

traces display a two-step mass loss in the 200−700 °C window and are represented by 1 and 2 in Figure 7. The slight mass loss below 200 °C is attributed to water. In spite of repeated vacuum drying, complete elimination of water was not possible. This is also reflected in the FT-IR spectra. The mass losses are centered around 250 and 400 °C, and it is likely that these correspond to the two different binding sites since there are two types of thiolates at the interface: 6 thiolates bridge Au(I) and 12 thiolates bridge Au(I) and Au(0) around the icosahedral Au_{13} core,[29] reflecting the asymmetry in the ligand structure. The calculated mass losses in the first and second steps are around 18% and 36%, which could be attributed to the desorption of 6 thiolates and 12 thiolates, respectively. Hence the mass loss corresponding to one thiolate comes around 3%. Unlike in the case of Au MPCs, no single mass loss is observed. Also, the mass loss is extending over a large window of temperature, suggesting processes other than simple desorption.[37,38] Continued heating from 200 to 700 °C results in the decomposition of the organics. An exothermic peak with a maximum at ∼500 °C is seen in differential thermal analysis (DTA) and could be attributed to oxidation of all the monolayers, and such an exothermic peak was not observed in the TG of mercaptosuccinic acid (MSA)-capped gold nanoparticles in N_2.[2] After 500 °C, only gold is expected to be present in the material as all the organics are decomposed. This was also confirmed by independent gravimetric experiments. TG was also performed in air to compare with the gravimetric experiments conducted in air. The observed weight percent of gold in $Au_{25}SG_{18}$ was 46%, which is in good agreement with the theoretical value (47%). Assuming the presence of water to the same extent and the retention of the Au_{25} core (as seen in UV−vis), the fraction of organics in $Au_{25}-MB$ and $Au_{25}-SGAN$ is 49 and 58%, respectively. This corresponds to a composition of $Au_{25}MB_5$-SG_{13} and $Au_{25}SGAN_{15}SG_3$ for these compounds. As ligand exchange can produce a distribution of molecular weights, we

consider these as the average compositions. This has been confirmed by the elemental analyses of $Au_{25}SG_{18}$, $Au_{25}-MB$, and $Au_{25}-SGAN$, and the data are given in the Supporting Information (Table 1). For compound $Au_{25}SG_{18}$, a mass loss of 54%, due to $(-SG)_{18}$, 1% higher than expected due to water as mentioned above, was measured. The compositions of $Au_{25}-MB$ and $Au_{25}-SGAN$ are different, as it appears that greater ligand exchange is possible for similar ligands (GSH and NAGSH).

$Au_{25}SG_{18}$ shows a characteristic emission in the solid state at 700 nm, comparable to the fluorescence maximum. Solid-state emission from molecular clusters of this kind has not been reported before. Spectral imaging of a drop casted film was done using this emission, which clearly shows the Au_{25}-rich region. These emissions are also observed in other clusters. For $Au_{25}-MB$, the emission is blue-shifted as shown in Figure 8, which is in agreement with the solution phase emission data. None of these compounds showed Raman features. It appears that Raman features were merged in the inherent fluorescence, because the later is much more intense. It is clear that the optical image (a) does not show features due to the clusters as clearly as in the fluorescence image (c).

We also studied the temperature dependence of the solid-state emission of $Au_{25}SG_{18}$ using the confocal Raman spectrometer (Figure 9). A solution of 10^{-3} M $Au_{25}SG_{18}$ was prepared, and it was drop casted on a thin glass plate and dried at room temperature. Experiments were carried out at various temperatures from 80 to 300 K at an interval of 10 K. At 80 K the emission intensity was very small and gradually increased with increasing temperature. Up to 160 K, the increment in intensity was small, and pronounced enhancement was observed only after 160 K. This is the first report on the temperature-dependent solid-state emission of molecular clusters. The emission occurs at the same position throughout the temperature window, indicating that there are no geometric changes in the

Ligand Exchange of Au₂₅SG₁₈

J. Phys. Chem. C, Vol. 112, No. 32, 2008 **12175**
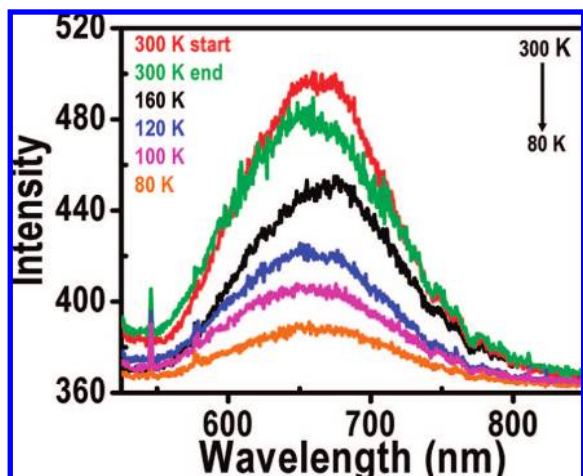
Figure 9. Temperature-dependent solid-state emission from $Au_{25}SG_{18}$. Note that the emission at 300 K almost retained its intensity even after a complete cycle of the experiment.

system affecting its electronic structure. We see that there is a weak asymmetry in the spectrum and the peak shape shows distinct changes as a function of temperature. This could be attributed to the open shell structure of the core and consequent structural distortion, but the Jahn−Teller effect in the system is expected to be small.[30] Coming to the decrease in the intensity of the fluorescence, the nonradiative relaxation channel becomes prominent with decrease in temperature. Although no explanation can be proposed, it suggests significant vibrational relaxation. However, no transition was detected in differential scanning calorimetry down to 173 K.

Summary and Conclusions

Application of the versatile ligand exchange methodology, practiced on MPCs, yield chemically similar molecular quantum clusters of gold. A variety of tools have been used to characterize the clusters; both the core and the ligand features were completely characterized. Optical absorption features are similar in all the clusters, confirming the results from the calculations. Ligand exchange reaction was monitored by ^{1}H NMR spectroscopy, and it is found that it follows a first order kinetics. The data also suggest that the exchange begins immediately and is complete within hours. Photoluminescence studies of these clusters, done in the aerated conditions, showed that the excitation spectrum of the MB-exchanged product is entirely different from the acetyl and formyl exchanged products. Thermogravimetric measurement was done in static air, and the data were used as a tool for computing the molecular weight of the exchanged products. The inherent fluorescence and solid-state emission of these clusters were observed, and this is the first report of this in this class of molecular clusters. This intense emission allows the optical imaging of the materials in the solid state. Solid-state emission from these clusters was found to be to temperature dependent and suggests hardening of phonons with decrease in temperature. The results presented here show the Au_{25} clusters with different functional modifications for diverse applications in areas such as energy transfer, sensors, biolabeling, and bioimaging are possible.

Supporting Information Available: TEM images of $Au_{25}SG_{18}$; ESI-MS mass spectrum of $Au_{25}SG_{18}$; expanded FT-IR of MB, Au_{25}−MB, NAGSH, and Au_{25}−SGAN; expanded ^{1}H NMR of GSH, $Au_{25}SG_{18}$, MB, Au_{25}−MB, NAGSH, Au_{25}−SGAN, NFGSH, and Au_{25}−SGFN; O1s and N1s core level photoelectron spectra of compounds, $Au_{25}SG_{18}$, Au_{25}−MB, and Au_{25}−SGAN and elemental analyses data of $Au_{25}SG_{18}$, Au_{25}−MB, and Au_{25}−SGAN. This material is available free of charge via the Internet at http://pubs.acs.org.

References and Notes

(1) Hostetler, M.; Wingate, J. E.; Zheng, C. J.; Harris, J. E.; Vachet, R. W.; Clark, M. R.; Londono, J. D.; Green, S. J.; Stokes, J. J.; Wignell, G. D.; Glish, G. L.; Porter, M. D.; Evans, N. D.; Murray, R. W. *Langmuir* **1998**, *14*, 17.
(2) Chen, S.; Kimura, K. *Langmuir* **1999**, *15*, 1075.
(3) Jana, N. R.; Gearheart, L.; Murphy, C. J. *J. Phys. Chem. B* **2001**, *105*, 4065.
(4) Sau, T. K.; Murphy, C. J. *J. Am. Chem. Soc.* **2004**, *126*, 8648.
(5) Millstone, J. E.; Park, S.; Shuford, K. L.; Mirkin, C. A. *J. Am. Chem. Soc.* **2005**, *127*, 5312.
(6) Ah, C. S.; Yun, Y. L.; Kim, W. L.; Ha, D. H.; Yun, W. S. *Chem. Mater.* **2005**, *17*, 5558.
(7) Yamamoto, M.; Kashiwagi, Y.; Sakata, T.; Nakamoto, M. *Chem. Mater.* **2005**, *17*, 5391.
(8) Sajanlal, P. R.; Pradeep, T. *Adv. Mater.* **2008**, *20*, 980.
(9) Schaaff, T. G.; Shafigullin, M. N.; Khoury, J. T.; Vezmar, I.; Whetten, R. L. *J. Phys. Chem. B* **1997**, *101*, 7885.
(10) Schaaff, T. G.; Knight, G.; Shafigullin, M. N.; Borkman, R. F.; Whetten, R. L. *J. Phys. Chem. B* **1998**, *102*, 10643.
(11) Chen, S.; Ingram, R. S.; Hostetler, M. J.; Pietron, J. J.; Murray, R. W.; Schaaff, T. G.; Khoury, J. T.; Alvarez, M. M.; Whetten, R. L. *Science* **1998**, *280*, 2098.
(12) Schwerdtfeger, P. *Angew. Chem., Int. Ed.* **2003**, *42*, 1892.
(13) Whetten, R. L.; Shaligullin, M. N.; Khouury, J. T.; Schaaff, T. G.; Vermar, I.; Alvarez, M. M.; Willkinson, A. *Acc. Chem. Res.* **1999**, *32*, 397.
(14) Huang, T.; Murray, R. W. *J. Phys. Chem. B* **2001**, *105*, 12498.
(15) Tsunoyama, H.; Sakurai, H.; Ichikuni, N.; Negishi, Y.; Tsukuda, T. *Langmuir* **2004**, *20*, 11293.
(16) Tsunoyama, H.; Sakurai, H.; Negishi, Y.; Tsukuda, T. *J. Am. Chem. Soc.* **2005**, *127*, 9374.
(17) Cui, Y.; Ren, B.; Jao, J. L.; Gu, R. A.; Tian, Z. Q. *J. Phys. Chem. B* **2006**, *110*, 4002.
(18) Bartlett, P. A.; Bauer, B.; Singer, S. *J. Am. Chem. Soc.* **1978**, *100*, 5085.
(19) Schmis, G.; Boese, R.; Pfeil, B.; Andermann, F.; Meyer, S.; Calis, G. H. M.; Van der Velden, J. W. A. *Chem. Ber.* **1981**, *114*, 3634.
(20) Zheng, J.; Petty, J. T.; Dickson, R. M. *J. Am. Chem. Soc.* **2003**, *125*, 7780.
(21) Zheng, J.; Zhang, C. W.; Dickson, R. M. *Phys. Rev. Lett.* **2004**, *93*, 077402.
(22) Negishi, Y.; Nobusada, K.; Tsukuda, T. *J. Am. Chem. Soc.* **2005**, *127*, 5261.
(23) Shichibu, Y.; Negishi, Y.; Tsukuda, T.; Teranishi, T. *J. Am. Chem. Soc.* **2005**, *127*, 13465.
(24) Shichibu, Y.; Negishi, Y.; Tsunoyama, H.; Kanehara, M.; Teranishi, T.; Tsukuda, T. *Small* **2007**, *3*, 835.
(25) Templeton, A. C.; Wuelfing, W. P.; Murray, R. W. *Acc. Chem. Res.* **2000**, *33*, 27.
(26) Bigioni, T. P.; Whetten, R. L. *J. Phys. Chem. B* **2000**, *104*, 6983.
(27) Lee, D.; Donkers, R. L.; Wang, G.; Harper, A. S.; Murray, R. W. *J. Am. Chem. Soc.* **2004**, *126*, 6193.
(28) Heaven, M. W.; Dass, A.; White, P. S.; Holt, k. M.; Murray, R. W. *J. Am. Chem. Soc.* **2008**, *130*, 3754.
(29) Akola, J.; Walter, M.; Whetten, R. L.; Hakkinen, H.; Groñbeck, H. *J. Am. Chem. Soc.* **2008**, *130*, 3756.
(30) Iwasa, T.; Nobusada, K. *J. Phys. Chem. C* **2007**, *111*, 45.
(31) Levy, E. J.; Anderson, M. E.; Meister, A. *Anal. Biochem.* **1993**, *214*, 135.
(32) Muhammed, M. A. H.; Pradeep, T. *Chem. Phys. Lett.* **2007**, *449*, 186.
(33) Tracy, J. B.; Kalyuzhny, G.; Crowe, M. C.; Balasubramanian, R.; Choi, J. P.; Murray, R. W. *J. Am. Chem. Soc.* **2007**, *129*, 6706.
(34) Schaaff, T. G.; Knight, G.; Shafigullin, M. N.; Borkman, R. F.; Whetten, R. L. *J Phys. Chem. B* **1998**, *102*, 10643.

12176 *J. Phys. Chem. C, Vol. 112, No. 32, 2008*

Shibu et al.

(35) Roger, H. T.; Timothy, A. P.; Chen, C. H.; Poon, C. D.; Andreas, T.; Chen, A.; James, E. H.; Michel, R. C.; George, W *J. Am. Chem. Soc.* **1995**, *117*, 12537.

(36) Wang, G.; Guo, R.; Kalyuzhny, G.; Choi, J. P.; Murray, R. W. *J. Phys.Chem B* **2006**, *110*, 20282.

(37) Sandhyarani, N.; Antony, M. P.; Panneer Selvam, G.; Pradeep, T. *J. Chem. Phys.* **2000**, *113*, 9794.

(38) Sandhyarani, N.; Resmi, M. R. ; Unnikrishnan, R.; Vidyasagar, K.; Ma, S.; Antony, M. P.; Panneer Selvam, G.; Visalakshi, V.; Chandra-kumar, N.; Pandian, K.; Tao, Y.-T.; Pradeep, T. *Chem. Mater.* **2000**, *12*, 104.